Mechanism and Tafel Lines of Electro-Oxidation of Water to Oxygen on RuO₂(110)

Ya-Hui Fang and Zhi-Pan Liu*

Shanghai Key Laboratory of Molecular Catalysis and Innovative Materials, Department of Chemistry, Key Laboratory of Computational Physical Science (Ministry of Education), Fudan University, Shanghai 200433, People's Republic of China

Received August 3, 2010; E-mail: zpliu@fudan.edu.cn

Abstract: How to efficiently oxidize H_2O to O_2 ($H_2O \rightarrow 1/2O_2 + 2H^+ + 2e^-$) is a great challenge for electrochemical/photo water splitting owing to the high overpotential and catalyst corrosion. Here extensive periodic first-principles calculations integrated with modified-Poisson−Boltzmann electrostatics are utilized to reveal the physical origin of the high overpotential of the electrocatalytic oxygen evolution reaction (OER) on RuO₂(110). By determining the surface phase diagram, exploring the possible reaction channels, and computing the Tafel lines, we are able to elucidate some long-standing puzzles on the OER kinetics from the atomic level. We show that OER occurs directly on an O-terminated surface phase above 1.58 V vs NHE, but indirectly on a OH/O mixed phase below 1.58 V by converting first the OH/O mixed phase to the O-terminated phase locally. The rate-determining step of OER involves an unusual water oxidation reaction following a Eley−Rideal-like mechanism, where a water molecule from solution breaks its OH bond over surface Os with concurrent new O−OH bond formation. The free energy barrier is 0.74 eV at 1.58 V, and it decreases linearly with the increase of potential above 1.58 V (a slope of 0.56). In contrast, the traditionally regarded surface oxygen coupling reaction with a Langmuir−Hinshelwood mechanism is energetically less favored and its barrier is weakly affected by the potential. Fundamentally, we show that the empirical linear barrier~potential relation is caused by the linear structural response of the solvated transition state to the change of potential. Finally, the general strategy for finding better OER anode is also presented.

1. Introduction

The electrolysis of water is regarded as a practical and green route for energy storage and conversion, which utilizes electric energy to split abundant water into clean fuel H_2.[1−4] Because the oxygen evolution reaction (OER) on an anode causes the major energy loss, better anode catalysts with low overpotential and long-term stability have been constantly pursued. While typical metal anode materials suffer severe drawbacks above the equilibrium potential of OER (1.23 V vs NHE), such as electrode corrosion and low current efficiency, the conductive rutile oxides, especially RuO₂, emerge as promising anode materials for OER. Although the doping/mixing of RuO₂ with many elements such as Ir,[2,5] Co,[6,7] Ce,[3,8] Pb,[9,10] and Ni[11,12] has been tested to improve OER performance, it remains elusive

how to design better OER anode catalysts, not least because the atomic-level picture on OER kinetics is not yet established.

Despite the lack of direct support, the microscopic mechanism of electrocatalytic OER was best regarded as a sequential mechanism via the stepwise decomposition of water, i.e., $H_2O \rightarrow OH + H^+ + e^- \rightarrow O + 2H^+ + 2e^-$ followed by an oxygen coupling reaction, $O + O \rightarrow O_2$. The kinetics model based on this mechanism has been utilized to rationalize the measured current~overpotential ($\log(j)\sim\eta$) plot, known as the Tafel line, which was commonly utilized for the assessment of the electrode performance for OER. There are two clear Tafel lines observed for OER on RuO₂, one at the lower potentials (e.g., < ~1.52 V) with a slope of 30−60 mV (i.e., 59 mV on RuO₂(110); 30−60 mV on RuO₂ particles) and another at the higher potentials with a slope of ~120 mV.[13,14] On the basis of the microkinetics analysis on RuO₂(110), Trasatti et al. suggested that the rate-determining step switches at ~1.52 V from the OH deprotonation step ($OH \rightarrow O + H^+ + e^-$) to the water splitting step ($H_2O \rightarrow OH + H^+ + e^-$) and the surface oxygen coupling step is not rate-limiting.[14] However, why the rate-

(1) Lim, B.; Jiang, M. J.; Camargo, P. H. C.; Cho, E. C.; Tao, J.; Lu, X. M.; Zhu, Y. M.; Xia, Y. A. *Science* **2009**, *324*, 1302.
(2) Ye, Z. G.; Meng, H. M.; Sun, D. B. *Electrochim. Acta* **2008**, *53*, 5639.
(3) Santana, M. H. P.; De Faria, L. A. *Electrochim. Acta* **2006**, *51*, 3578.
(4) Winther-Jensen, B.; Winther-Jensen, O.; Forsyth, M.; MacFarlane, D. R. *Science* **2008**, *321*, 671.
(5) Di Blasi, A.; D'Urso, C.; Baglio, V.; Antonucci, V.; Arico, A. S.; Ornelas, R.; Matteucci, F.; Orozco, G.; Beltran, D.; Meas, Y.; Arriaga, L. G. *J. Appl. Electrochem.* **2009**, *39*, 191.
(6) Da Silva, L. M.; Boodts, J. F. C.; De Faria, L. A. *Electrochim. Acta* **2001**, *46*, 1369.
(7) Jirkovsky, J.; Makarova, M.; Krtil, P. *Electrochem. Commun.* **2006**, *8*, 1417.
(8) Fernandes, K. C.; Da Silva, L. M.; Boodts, J. F. C.; De Faria, L. A. *Electrochim. Acta* **2006**, *51*, 2809.
(9) Musiani, M.; Furlanetto, F.; Bertoncello, R. *J. Electroanal. Chem.* **1999**, *465*, 160.
(10) Bertoncello, R.; Cattarin, S.; Frateur, I.; Musiani, M. *J. Electroanal. Chem.* **2000**, *492*, 145.
(11) Macounova, K.; Jirkovsky, J.; Makarova, M. V.; Franc, J.; Krtil, P. *J. Solid State Electrochem.* **2009**, *13*, 959.
(12) Macounova, K.; Makarova, M.; Jirkovsky, J.; Franc, J.; Krtil, P. *Electrochim. Acta* **2008**, *53*, 6126.
(13) Guerrini, E.; Trasatti, S. *Russ. J. Electrochem.* **2006**, *42*, 1017.
(14) Castelli, P.; Trasatti, S.; Pollak, F. H.; Ogrady, W. E. *J. Electroanal. Chem.* **1986**, *210*, 189.

determining step switches particularly at ∼1.52 V remains puzzling considering that a number of factors may be the cause, such as the surface morphology change or the variation of reaction mechanism.[15-17]

Furthermore, this simple sequential OER mechanism does not sit comfortably on recent theoretical findings concerning the O—O bond formation channel. Using density functional theory (DFT) calculations, Nørskov and co-workers[18] have investigated the thermodynamics for OER on three rutile (110) surfaces, namely TiO_2, RuO_2, and IrO_2, and the electrochemical effects were simplified by a first-order term to account for the free energy change of proton and electron under potentials. It was shown that the OOH intermediate is generally less stable than adsorbed O and OH and the formation of OOH was proposed to be the key step in OER. With a Gaussian-plane-charge method to take into account the surface polarization under electrochemical conditions, our recent results for OER on Pt surfaces showed that the oxygen coupling (O + O) reaction is kinetically less favorable compared to the O + OH reaction, where the formation of the O—O bond requires a high potential and involves the surface stepped sites.[19] However, the formation of OOH via O + OH being the rate-determining step is apparently inconsistent with the experimental explanation for Tafel lines. Indeed, we also found that the barriers of O + O and O + OH reactions on Pt surfaces are marginally affected by the applied electric fields, exhibiting a non Tafel-line behavior.[19]

To better understand electrocatalytic phenomena in general, a unified theoretical framework for treating electrocatalytic kinetics reliably is now urgently called for. Recent years have seen a number of theoretical groups working on the quantum mechanics modeling of electrocatalytic reactions.[20-23] Taking the OER kinetics on $RuO_2(110)$ as the model system, here we combine periodic first-principles calculations with a numerical modified-Poisson—Boltzmann solver for electrostatics to investigate how OER occurs under the influence of the electrochemical potential and the aqueous surroundings. We identify a new mechanism for OER on $RuO_2(110)$ and rationalize quantitatively the concerned high overpotential. With the Tafel lines computed from first principles, we are able to establish a quantum mechanics basis for the linearity and slope of Tafel lines in general. Finally, how to find a better OER anode is also addressed by comparing three different materials, i.e., Pt, RuO_2, and IrO_2.

2. Methodology and Calculations

2.1. DFT Calculations. All DFT calculations were performed using the SIESTA package with numerical atomic orbital basis sets and Troullier—Martins normconserving pseudopotentials.[24-26] The exchange-correlation functional utilized was at the generalized gradient approximation level, known as GGA-PBE.[27] A double-ξ plus polarization basis set was employed for the valence state and the orbital-confining cutoff was determined from an energy shift of 0.010 eV. The energy cutoff for the real space grid used to represent the density was set as 150 Ry. For Ru (Ir), the semicore $4s^24p^6$ ($5s^25p^6$) states were included, which were found to be essential for the description of oxides. The Broyden method was employed for geometry relaxation until the maximal forces on each relaxed atom were less than 0.1 eV/Å. To correct the zero-point-energy (ZPE), the vibrational frequency calculations were performed via the finite-difference approach. The $RuO_2(110)$ surface was routinely modeled by p(3 × 1) [9.27 × 6.39 Å] unit cell in a symmetric six-layer slab (in total $Ru_{36}O_{72}$, each layer contains a trilayer RuO_2 unit) with the middle two layers being fixed at the bulk-truncated position. Spin polarized calculations have been performed for systems involving molecular O_2 adsorption and the spin polarization affects the adsorption energetics in a rather small manner (<0.03 eV), as reported in previous DFT calculations.[28] The Monkhorst-Pack type of k-point sampling with a (2 × 3 × 1) mesh was used for all p(3 × 1) slab calculations and the denser (3 × 4 × 1) k-point mesh was used to further check the convergence of reaction energetics (see Supporting Information, SI, Table S-1). To construct the surface diagram of $RuO_2(110)$, in particular at low coverage conditions, a larger p(6 × 1) slab with three RuO_2 trilayers was utilized with a (1 × 3 × 1) Monkhorst-Pack k-point mesh. The accuracy of the calculated energetics was examined by benchmarking the results from SIESTA with those from the plane-wave methodology. For example, the O atom free energy of adsorption (with respect to the free energy of the gas phase O_2 at the standard state, $G(O_2)$) on $RuO_2(110)$ is calculated to be −0.63 eV from SIESTA, and it is −0.65 eV from plane-wave method in a p(1 × 1) unit cell. Transition states (TSs) of the catalytic reaction were searched using the Constrained-Broyden-Minimization[29] and the Broyden-Dimer method.[30]

To derive the free energy reaction profile, we first obtain the reaction energy of each elementary step (strictly, ΔF at 0 K, 0 bar), which is directly available from DFT total energy (ΔE) after the ZPE correction. For elementary surface reactions without involving the adsorption/desorption of gaseous or liquid molecules, ΔF at 0 K, 0 bar is a good approximation to the Gibbs free energy (ΔG) as the temperature T and pressure p contributions at solid phase are small. To compute the free energy change ΔG of elementary reactions involving gaseous or liquid molecules, such as oxygen, hydrogen, and water, it is essential to take into account the large entropy term at 298 K. We utilize the standard thermodynamic data[31] to obtain the temperature and pressure contributions for the G of the aqueous H_2O and gaseous H_2, which are −0.57 eV (the entropy contribution is −0.22 eV in solution) and −0.31 eV compared to the total energy of the corresponding free molecule (E, 0 K), respectively.[32] The G of O_2 is derived as $G[O_2] = 4.92$ (eV) $+ 2G[H_2O] - 2G[H_2]$ by utilizing OER equilibrium at the

(15) Bockris, J. O. M. *J. Chem. Phys.* **1956**, *24*, 817.
(16) Damjanov, A.; Dey, A.; Bockris, J. O. M. *Electrochim. Acta* **1966**, *11*, 791.
(17) Santana, M. H. P.; De Faria, L. A.; Boodts, J. F. C. *Electrochim. Acta* **2004**, *49*, 1925.
(18) Rossmeisl, J.; Qu, Z. W.; Zhu, H.; Kroes, G. J.; Norskov, J. K. *J. Electroanal. Chem.* **2007**, *607*, 83.
(19) Fang, Y. H.; Liu, Z. P. *J. Phys. Chem. C* **2009**, *113*, 9765.
(20) (a) Rossmeisl, J.; Logadottir, A.; Norskov, J. K. *Chem. Phys.* **2005**, *319*, 178. (b) Rossmeisl, J.; Norskov, J. K.; Taylor, C. D.; Janik, M. J.; Neurock, M. *J. Phys. Chem. B* **2006**, *110*, 21833.
(21) (a) Filhol, J. S.; Neurock, M. *Angew. Chem., Int. Ed.* **2006**, *45*, 402. (b) Taylor, C. D.; Wasileski, S. A.; Filhol, J. S.; Neurock, M. *Phys. Rev. B* **2006**, *73*, 165402.
(22) (a) Jinnouchi, R.; Anderson, A. B. *Phys. Rev. B* **2008**, *77*, 245417. (b) Anderson, A. B.; Albu, T. V. *J. Am. Chem. Soc.* **1999**, *121*, 11855.
(23) (a) Jacob, T.; Goddard, W. A. *ChemPhysChem* **2006**, *7*, 992. (b) Goddard, W. A.; Merinov, B.; Van Duin, A.; Jacob, T.; Blanco, M.; Molinero, V.; Jang, S. S.; Jang, Y. H. *Mol. Simul.* **2006**, *32*, 251.

(24) Soler, J. M.; Artacho, E.; Gale, J. D.; Garcia, A.; Junquera, J.; Ordejon, P.; Sanchez-Portal, D. *J. Phys.: Condens. Matter* **2002**, *14*, 2745.
(25) Junquera, J.; Paz, O.; Sanchez-Portal, D.; Artacho, E. *Phys. Rev. B* **2001**, *64*, 235111.
(26) Troullier, N.; Martins, J. L. *Phys. Rev. B* **1991**, *43*, 1993.
(27) Perdew, J. P.; Burke, K.; Ernzerhof, M. *Phys. Rev. Lett.* **1996**, *77*, 3865.
(28) Wang, H. Y.; Schneider, W. F.; Schmidt, D. *J. Phys. Chem. C* **2009**, *113*, 15266.
(29) Wang, H. F.; Liu, Z. P. *J. Am. Chem. Soc.* **2008**, *130*, 10996.
(30) Shang, C.; Liu, Z. P. *J. Chem. Theory Comput.* **2010**, *6*, 1136.
(31) *CRC Handbook of Chemistry and Physics*, 84th ed.; Lide, R. D., Ed.; CRC Press: New York, 2003−2004.

standard conditions. For reactions involving the release of protons and electrons, the reaction free energy can be computed by referencing to NHE as suggested by Bockris[33] and Nørskov[20] groups. This is governed by $G_{proton+electron} = G_{1/2H2(g)} - neU$ where e presents the transfer electron and U is electrochemical potential.
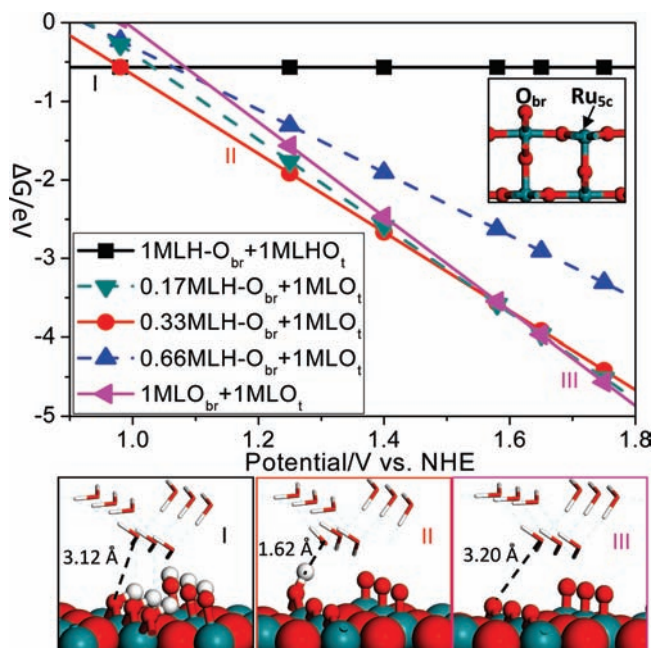
2.2. Modified Poisson–Boltzmann Approach for Electrochemistry. In our previous work, we have developed a Gaussian-plane-charge method for the calculation of charged surfaces[19] (the counter-charge is distributed in a Gaussian-plane several angstroms away from the surface), which considers the surface polarization explicitly due to the surface charging. However, because of the lack of solvation and the unrealistic ionic charge distribution, the Gaussian-plane-charge method is not ideal for an accurate description of electrocatalytic reaction. In this work, we replace the Gaussian-plane charge distribution by a point-charge distribution in the continuum dielectric medium,[22,34] which mimics the real ionic distribution of electrolyte. The continuum dielectric medium is introduced via a smooth dielectric function $\varepsilon(r)$ as proposed by Fattebert and Gygi,[35] which approaches ε_∞ (e.g., 78.36 for water at room temperature) asymptotically in the regions where electron density is low, and 1 in the regions where it is high. We utilize the modified Poisson–Boltzmann (MPB) equation shown in eq 1[36,37] to determine the total electrostatic potential, where $\beta = k_B T$ and $\varphi_0 = 2a^3 c_b$ (a is the effective ion size and c_b is the bulk concentration of the electrolyte). The Boltzmann distribution of the ionic charge (i.e., countercharge) is determined by the second term in the right-hand side of eq 1, which can be solved self-consistently during electronic structure loops (a representative result for the distribution of the ionic countercharge is shown in the SI Figure S-1). In this work, φ_0 is set as 2×10^{-3} by assuming $c_b = 0.1$ mol/L, $a = 2-4$ Å and $z = 1$ for typical 1:1 electrolytes.[36] The technique detail for the implementation of the numerical PB solver in periodic slab calculations was described in our previous work[34,38] and the MPB solver utilized in this work is a parallel version of MINRES with the preconditioner.

$$\nabla \cdot (\varepsilon(r) \nabla \Psi) = -4\pi\rho + 8\pi z e c_b \frac{\sinh(z\beta e\Psi)}{1 - \varphi_0 + \varphi_0 \cosh(z\beta e\Psi)} \tag{1}$$

$$U_{cal}^q = (\Psi_{ref} - \Psi_F) - 4.6 \tag{2}$$

$$\eta = U_{cal}^q - (U_{cal}^0 - U_p) - 1.23 \tag{3}$$

With the MPB solver, we can calculate the electrochemical potential U_{cal}^q of a system with a net charge q referring to NHE (work function 4.6 eV from experiment) using eq 2, where the computed work function in solution is defined as the potential difference between the Fermi Level Φ_F and the potential level in solution Φ_{ref}. Electrochemical potentials mentioned in this work are always referred to NHE. Next, eq 3 is utilized to compute the overpotential η that is required for Tafel plot, where we first offset U_{cal}^q by the difference between the U_{cal}^0 (neutral slab) at a particular surface phase **A** and the emergence potential (where the phase transition occurs) for the phase **A** obtained from surface phase diagram by DFT (U_p), and then subtract it by 1.23 V, the equilibrium potential of OER. For example, on Pt(111), 0.33 ML

(32) Liu, Z. P.; Jenkins, S. J.; King, D. A. *J. Am. Chem. Soc.* **2004**, *126*, 10746.
(33) Bockris, J. O. M.; Khan, S. U. M. *Surface Electrochemistry: A Molecular Level Approach*; Plenum Press: New York, 1993.
(34) Wang, H. F.; Liu, Z. P. *J. Phys. Chem. C* **2009**, *113*, 17502.
(35) Fattebert, J. L.; Gygi, F. *J. Comput. Chem.* **2002**, *23*, 662.
(36) Kilic, M. S.; Bazant, M. Z.; Ajdari, A. *Phys. Rev. E* **2007**, *75*, 021503.
(37) Borukhov, I.; Andelman, D.; Orland, H. *Phys. Rev. Lett.* **1997**, *79*, 435.
(38) (a) Fang, Y. H.; Liu, Z. P. *J. Phys. Chem. C* **2010**, *114*, 4057. (b) Li, Y. F.; Liu, Z. P.; Liu, L.; Gao, W. *J. Am. Chem. Soc.* **2010**, *132*, 13008.

Figure 1. The surface phase diagram of RuO₂(110) and the optimized structures of the three stable surface phases. Phase I: the OH-terminated phase (1 ML H–O$_{br}$ + 1 ML HO$_t$); phase II: the 0.33 ML H–O$_{br}$/O$_t$ mixed phase (0.33 ML H–O$_{br}$ + 1 ML O$_t$); and phase III: the O-terminated phase (1 ML O$_{br}$ + 1 ML O$_t$). The inserts show the surface structures of a bare RuO₂(110) (upright corner). O: Red ball; H: white ball; Ru: Green ball.

O coverage appears only above 0.7 and 0.7 V is defined as U_p for 0.33 ML O phase.[19] The offset is to cancel the systematic errors in the calculated absolute electrochemical potential from the DFT-MPB approach. The utilization of U_p from the surface phase diagram as an internal reference is based on the fact that the surface phase diagram is mainly dictated by thermodynamics and is insensitive to the explicit surface charging. We have shown that the surface phase diagram of Pt from Gaussian-plane-charge method and the simple thermodynamics method as suggested by Nørskov group are essentially the same.[19]

3. Results

3.1. Surface Phase Diagram of RuO₂(110). Before the investigation of kinetics, it is essential to know first the surface phase of RuO₂ at the OER condition. For bare RuO₂(110), there are two types of coordination unsaturated sites, namely the bridging O (O$_{br}$) and the five-coordinated Ru (Ru$_{5c}$) (see Figure 1 insert). In electrochemical conditions, the O$_{br}$ can accept H from H₂O, and H₂O, OH and O can adsorb on the top of Ru$_{5c}$. Our calculations showed that water dissociation at a vacant Ru$_{5c}$ site of RuO₂ can occur easily as the calculated barrier is very low (<0.2 eV), in consistent with previous work,[39,40] which implies that the surface phase of RuO₂ is dictated by thermodynamics at room temperature.

We therefore explored the adsorption of H₂O, O, H, and OH species at different coverages and each is considered to be a possible surface phase. The calculated free energy of adsorption (ΔG per p(3 × 1) unit cell) with respect to the bare surface and water were utilized to construct the surface phase diagram by

(39) Knapp, M.; Crihan, D.; Seitsonen, A. P.; Over, H. *J. Am. Chem. Soc.* **2005**, *127*, 3236.
(40) Knapp, M.; Crihan, D.; Seitsonen, A. P.; Resta, A.; Lundgren, E.; Andersen, J. N.; Schmid, M.; Varga, P.; Over, H. *J. Phys. Chem. B* **2006**, *110*, 14007.

using the method addressed in our previous work.[19] Due to a large number of possible surface phases, in practice, we adopted a two-step procedure to identify the surface phase diagram under the electrochemical environment. First, the possible phases of H_2O, O, and OH species (in total 19 phases considered) in vacuum was calculated, and by constructing the surface diagram in vacuum the least stable phases were screened, as shown in SI Figures S-2 and S-3. We found that the fully OH-terminated phase (at low potentials), several mixed OH/O termination phases with H on O_{br} and a 1 ML of O_t on Ru_{5c} (at intermediate potentials) and a fully O-terminated phase (at high potentials) are among the most sable phases. The coverage (ML) here is with respect to the number of exposed Ru_{5c}. Next, to obtain more realistic phase diagram in solution, we then added the explicit water layer as the first solvation shell together with the continuum solvation model to include the long-range electrostatic solvation effect, and recalculated the energetics of the most stable phases known from the vacuum results, including the fully OH-terminated phase, the O-terminated phase, and three OH/O mixed phases. The obtained surface diagram in aqueous surroundings (in the presence of first shell water and the continuum solvation) is shown in Figure 1.

It might be mentioned that the water layer on $RuO_2(110)$ as explicit solvent is to take into account the specific interaction between the adsorbed species (H, OH, and O) and the first water shell. This is crucial for obtaining a correct kinetics description of OER, as will be demonstrated later. Due to the protruding nature of O_{br} on (110) surface, it is not possible to form a flat water layer on the surface,[41] instead we adopted three rows of H_2O as the first water layer that are interlinked by H-bondings with only the bottom row of H_2O being directly in contact with surface (see Figure 1).

As shown in Figure 1, an OH-terminated surface is the most stable phase at low potentials, which can be viewed as a clean $RuO_2(110)$ covered by a full layer of dissociated H_2O with H on O_{br} and HO on Ru_{5c}. Above the phase-transition potential 1.58 V, a fully oxygen-terminated phase is preferred thermodynamically, where each Ru_{5c} is coordinated with a terminal O (O_t). These two phases were identified previously by DFT combined with thermodynamics where a smaller p(2 × 1) unit cell was utilized.[18] Importantly, this work reveals a new phase in between 1.0 and 1.58 V, which features a mixed OH/O termination with 1/3 (0.33) ML H on O_{br} and 1 ML of O_t on Ru_{5c} (denoted as 0.33 ML $H-O_{br}/O_t$ phase). It is also noticed that the free energy of the phase with 0.17 ML HO_{br} and 1 ML of O_t on Ru_{5c} is in between those of the 0.33 ML $H-O_{br}/O_t$ phase and the fully O-terminated phase, and near the phase-transition potential (around 1.6 V) all three phases are close in energy. This implies that it is in fact feasible to have a finite coverage of H (i.e $H-O_{br}$ ≤0.33 ML) at this potential range thermodynamically according to Boltzmann distribution. The close-in-energy of several phases near the phase-transition potential here on RuO_2 is rather similar to what was found previously in the surface phase diagram of Pt surfaces.[19] For the concern of OER activity, the 0.33 ML $H-O_{br}/O_t$ phase and the O-terminated phase are of significance, which represent the two limiting surface conditions. Without specific mentioning, the OH/O mixed phase hereafter is always referred to the 0.33 ML $H-O_{br}/O_t$ phase.

We noticed that the stability of the fully OH-terminated and the O-terminated surface are little affected (0.07 and 0.02 eV

(41) Chu, Y. S.; Lister, T. E.; Cullen, W. G.; You, H.; Nagy, Z. *Phys. Rev. Lett.* **2001**, *86*, 3364.
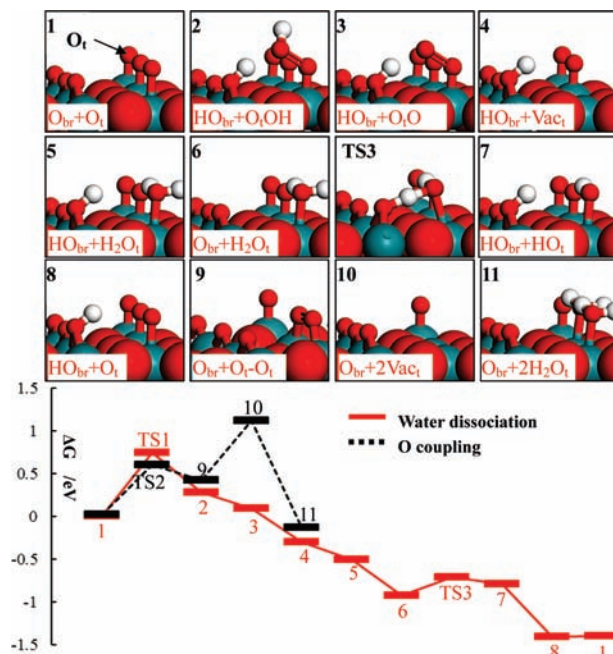
Figure 2. The optimized structures of intermediate states and the free energy profile for OER on the O-terminated phase of $RuO_2(110)$ at 1.58 V. O_{br}, O_t, and Vac_t are the bridging O, the terminal O on Ru_{5c} and the vacant Ru_{5c} site, respectively. For the optimized structures, the first H_2O layer is omitted for clarity. O: Red ball; H: white ball; Ru: Green ball.

per p(3 × 1) cell[18] by the water layer and the continuum solvation since the optimized distance between the first layer water and the surface is quite long (>3 Å as shown in Figure 1). For the OH/O mixed phase, however, the $H-O_{br}$ can interact strongly with the first layer water as evident by a short H-bonding length ($O_{br}H---OH_2$, 1.62 Å), which is apparently due to the strong acidity of the $H-O_{br}$ group. Our calculations show that the HO/O mixed phase is stabilized by 0.41 eV in the presence of the explicit water layer and the continuum solvation compared to it in vacuum. Therefore, the presence of the OH/O mixed phase at intermediate potentials can be attributed both to its intrinsic stability (as shown in Figure S-3 of the SI) and also to the strong solvation effect.

3.2. OER Kinetics. 3.2.1. On the O-Terminated Phase (>1.58 V). On the basis of the phase diagram, we are now able to model OER at a particular electrochemical potential with a known precoverage of surface oxidative species. We initiated our investigation from the O-terminated phase (i.e., >1.58 V), which has a relatively simple surface structure and is also the most relevant to OER activity in experiment. We have identified two possible reaction channels toward oxygen evolution on this phase, and according to their initiating step, we named the two reaction channels as the water dissociation path and the surface oxygen coupling path. The computed key reaction intermediates are highlighted in Figures 2 and 3. The data for computing the reaction free energy at 1.58 V is summarized in Table 1 and the reaction profile is plotted in Figure 2.

The water dissociation path is the lowest energy pathway (Figure 2 red-solid line). Following a Eley−Rideal (ER)-like mechanism, the reaction starts by the dissociation of a water molecule over two surface Os, O_t, and O_{br} (state **1**, Figure 2). The calculated free energy barrier is 0.74 eV in the presence of the first layer water. At the TS (**TS1**, Figure 3), the water passes its H to O_{br} and the left OH evolves a bonding with O_t-Ru_{5c}, which finally yields a $H-O_{br}$ and a HOO_t-Ru_{5c} (state **2**, with
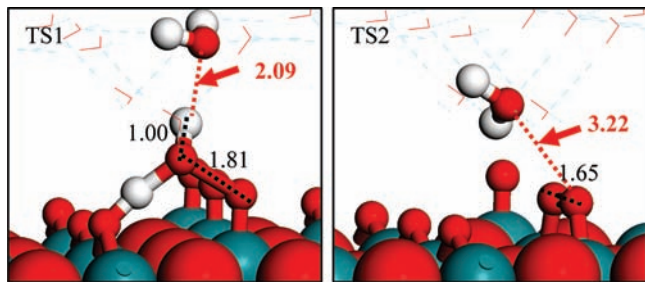
Figure 3. TS structures of the water dissociation (TS1) and surface oxygen coupling (TS2) on the O-terminated phase of $RuO_2(110)$. All of the distances labeled are in Angstrom. O: Red ball; H: White ball; Ru: Green ball.

Table 1. Calculated Free Energies of Elementary Steps in OER on the O-Terminated Phase of $RuO_2(110)^a$

elementary steps	ΔE	$\Delta H(0{\to}298K)$	ΔZPE	$-T\Delta S$	$-|e|U$	ΔG
water dissociation path						
$1 \to TS1$	0.59	0	−0.07	0.22	0	0.74
$1 \to 2$	0.03	0	0.03	0.22	0	0.28
$2 \to 3 + H^+ + e^-$	1.68	0.04	−0.15	−0.2	−1.58	−0.20
$3 \to 4 + O_2$	0.25	0.09	−0.08	−0.64	0	−0.38
$4 + H_2O \to 5$	−0.59	0	0.17	0.22	0	−0.20
$5 \to 6 + H^+ + e^-$	1.53	0.04	−0.21	−0.2	−1.58	−0.42
$6 \to TS3$	0.21	0	0	0	0	0.21
$6 \to 7$	0.16	0	−0.03	0	0	0.13
$7 \to 8 + H^+ + e^-$	1.36	0.04	−0.23	−0.2	−1.58	−0.61
$8 \to 1 + H^+ + e^-$	1.95	0.04	−0.21	−0.2	−1.58	0.01
oxygen coupling path						
$1 \to TS2$	0.50	0	0.1	0	0	0.60
$1 \to 9$	0.32	0	0.1	0	0	0.42
$9 \to 10 + O_2$	1.41	0.09	−0.16	−0.64	0	0.70
$10 + 2H_2O \to 11$	−2.03	0	0.34	0.44	0	−1.25

a The structures of the states labeled from **1** to **11** are shown in Figure 2. $\Delta H(0 \to 298 K)$ is deduced from ref 31.

Table 2. Calculated Bader Net Charge (Q, |e|) for the Water Dissociation and the Surface Oxygen Coupling Reactions on the O-Terminated Phase of $RuO_2(110)$ from the Initial State (IS) to the Transition State (TS) and to the Final State (FS)

reaction	species	IS	TS	FS
water dissociation	$(H_2O)_{n-1}^{Solv}$	+0.10	+0.11	+0.16
	H_2O^{Reac}	+0.02	+0.82	+1.09
	$Surf^a$	−0.12	−0.93	−1.25
O coupling	$(H_2O)_n^{Solv}$	+0.11	+0.12	+0.10
	$[O_t-O_t]$	−0.99	−0.72	−0.50
	$Surf^a$	−0.10	−0.12	−0.10

a The O-terminated phase of $RuO_2(110)$ (including all O_t atoms).

a O−OH distance 1.42 Å). By using Bader charge analysis as listed in Table 2, we found that the dissociating water (H_2O^{Reac}) donate electrons to the surface during the reaction, leading to the formation of a protonated peroxo [OOH] complex at the final state (FS). The net charge on the dissociating water is 0.82 and 1.09 |e| at the TS and the FS, respectively, while it is only 0.02 |e| at the initial state (IS). The other water molecules in the first solvation shell [$(H_2O)_{n-1}^{solv}$] maintains a quite constant net charge of +0.1 |e|, indicating that the solvation helps to stabilize the [O−OH] complex mainly through the H-bonding with no significant charge transfer.

Next, the H on HOO−Ru_{5c} is released as a proton to solution to yield an adsorbed OO−Ru_{5c} (state **3**). The proton transfer from HOO−Ru_{5c} to solution is a facile step as shown by the first principles molecular dynamics (MD) simulation. We performed a Nose thermostat MD starting from state **2** at 330 K ($\Delta t = 1$ fs) with three-layer water on the surface. The MD simulation shows that the proton transfer from HOO−Ru_{5c} to

the water layers occurs within ~0.5 ps, yielding a $H_5O_2^+$ in solution and an adsorbed O_2 on the surface (shown in the SI Figure S-4). The final state with $H_5O_2^+$ in solution is then calculated by geometry optimization and it is found that the proton transfer is exothermic by 0.31 eV. From state **3** to state **4**, it is a O_2 molecule releasing to free a vacant Ru_{5c} site, where a new-coming H_2O molecule can then adsorb with 0.94 eV adsorption energy (state **5**). The subsequent steps are the step-wise deprotonation from the H−O_{br} (**5 → 6**) and from the dissociated water (**7 → 8 → 1**), which finally restores the O-terminated phase. The second water dissociation step (**6 → TS3**) has only a 0.21 eV reaction barrier, while the other proton releasing steps (**5 → 6, 8 → 1**) are generally exothermic and are believed to be facile at the high potentials.

In parallel to the water dissociation pathway, we also revealed that the surface oxygen atoms, e.g., O_t, can recombine first to release O_2 with a Langmuir−Hinshelwood (LH) mechanism. The direct oxygen coupling step was proposed and widely referred in experiment.[3,7,42,43] In the oxygen coupling pathway, the O_t on Ru_{5c} reacts with each other (**TS2**, Figure 3) by overcoming a reaction barrier of 0.60 eV in the presence of the first layer water (see Table 1). Distinct from the water dissociation reaction, there is marginal net electron transfer from the outer water layer to the surface during the surface oxygen coupling reaction. The net charges on the water layer and the surface are rather constant, ~0.1 |e| as shown by the Bader charge analysis in Table 2. The reacting [O_t-O_t] (also a part of the surface) become increasingly less negatively charged (from −0.99 to −0.72 and to −0.50 |e|) on going from IS to TS and to FS, which is compensated by the electron density increase on surface Ru_{5c} atoms.

The adsorbed O_2 molecule on two Ru_{5c} sites is quite stable and its desorption (**9 → 10**) is energetically unfavorable. The overall free energy barrier is 1.1 eV on going from two O_t to a gas phase O_2. This is to a large extent due to the high free adsorption energy of O (−0.40 eV at 1 ML and −0.81 eV at 0.67 ML for adsorbed O_t), which will be discussed in detail in the section 4.2. It might be mentioned that we also considered the possibility of oxygen coupling between O_{br} and O_t (as shown in SI Table S-2). The reaction channel can also be ruled out due to the high reaction barrier (0.90 eV). Overall, the surface oxygen coupling path above 1.58 V is unlikely due to the difficulty of O_2 releasing from Ru_{5c} sites.

3.2.2. On the HO/O Mixed Phase (<1.58 V). We have identified three OER reaction routes on the HO/O mixed phase, namely the water dissociation path, the oxygen coupling path and the deprotonation path, as distinguishable by their initiating step. The first two paths are similar to their counterparts on the O-terminated phases except there is 0.33 ML H at the O_{br} (as shown in SI Figure S-5), while the deprotonation path starts from the proton releasing of H−O_{br}. The overall free energy diagram of the pathways at 1.4 V is plotted in Figure 4. Among the three pathways, the deprotonation path is the lowest energy pathway. The initial deprotonation of H−O_{br} effectively converts the HO/O mixed phase to the O-terminated phase locally. At 1.4 V, the free energy change for the deprotonation step (**8 → 1**) is only 0.20 eV in the p(3 × 1) unit cell. After the proton removal, the subsequent path resembles the water dissociation path on the O-terminated phase as elaborated above.

(42) Santana, M. H. P.; De Faria, L. A.; Boodts, J. F. C. *Electrochim. Acta* **2005**, *50*, 2017.

(43) Jirkovsky, J.; Hoffmannova, H.; Klementova, M.; Krtil, P. *J. Electrochem. Soc.* **2006**, *153*, E111.
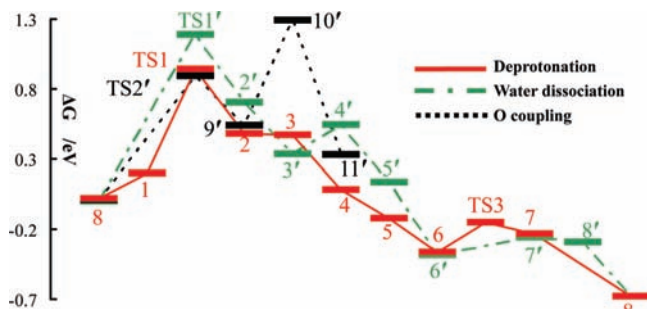
Figure 4. Free energy profile for OER on the 0.33 ML H—O$_{br}$/O$_t$ phase of RuO$_2$(110) at 1.40 V. **X'** is similar to **X** shown in Figure 2 and 3 except for the 0.33 ML H on O$_{br}$.
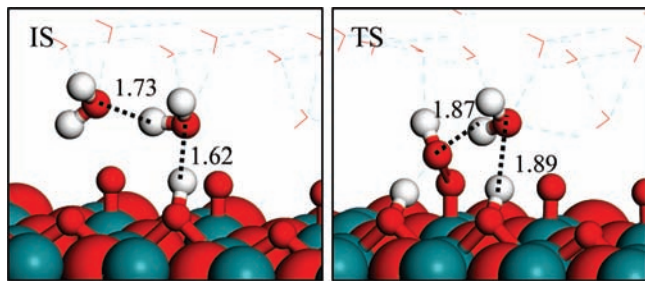
Figure 5. The optimized IS and TS structures for the direct dissociation of water at the 0.33 ML H—O$_{br}$/O$_t$ phase.

The other two paths are kinetically hindered by high free energy barriers (more than 1.1 eV). Since the 0.33 ML H at the O$_{br}$ is intact during the reactions of the two paths, the intermediate states of the two paths are very similar to those occurring on the O-terminated phase except the 0.33 ML H at O$_{br}$. These intermediate states are therefore denoted as X', where X are the states shown in Figure 2 and Figure 3. The water dissociation path is initiated by the direct dissociation of a water molecule over two surface Os, O$_t$, and O$_{br}$. Owing to the presence of 0.33 ML of H—O$_{br}$ at the OH/O mixed phase, the water dissociation becomes much more difficult with the calculated reaction barrier as high as 1.19 eV (**8 → TS1'**). By comparing the structure at the IS and the TS, we found that the high barrier can be mainly attributed to the solvation effect (as shown in Figure 5). The H—O$_{br}$ can form a strong H-bonding with a first layer water at the IS, while this H-bonding is much weakened at the TS when another neighboring water dissociates. For the oxygen coupling path on the OH/O mixed phase (**8 → 11'**), it is also kinetically hindered with the overall free energy barrier being more than 1.2 eV (**8 → 10'**) for two O$_t$ at the Ru$_{5c}$ to recombine and desorb.

3.3. Potential∼Barrier Relationship and Tafel Lines. We are now at the position to examine how the variation of the electrochemical potential can influence directly the barrier of key elementary reactions. For the OER on the O-terminated phase, the water dissociation step (**1 → 2**) is the rate-determining step because the TS of the step dictates the height of the potential energy surface. To analyze the potential dependence of the reaction barrier of this step, we have calculated the reaction at different surface charge conditions, namely −0.2, −0.1, −0.05, 0, +0.1, +0.2, +0.3, +0.4 |e| using a symmetric slab with the reaction occurring on both sides of the slab. The calculated barriers (E$_a$) are 0.65, 0.62, 0.62, 0.59, 0.53, 0.42, 0.35, and 0.26 eV at the set of surface charges. It is interestingly noticed that only at the positive surface charge conditions the reaction barriers changes dramatically. Next, we need to link the
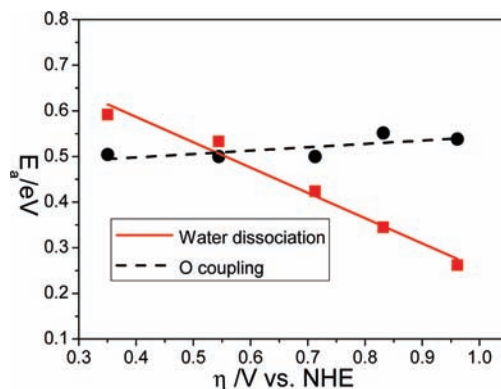

Figure 6. The plot of reaction barrier E$_a$ against the overpotential η for the water dissociation and the surface oxygen coupling on the O-terminated phase of RuO$_2$(110).

computed surface charge with the electrochemical potential since the electrochemical reaction is performed under a constant potential instead of the constant surface charge. By using eqs 2 and 3 where the U$_p$ is 1.58 V (an overpotential of 0.35 V) according to the phase diagram in Figure 1a, we were able to derive the overpotential of the charged systems at the IS, which are −0.12, 0.09, 0.27, 0.35, 0.54, 0.71, 0.83, and 0.96 V. In this work, we assume the electrochemical potential at the TS is the same as that at that of IS, considering that (i) the chemical reaction is a rare event and the occurrence of a single reaction on surface should not change the potential of the whole system, and (ii) the unit cell utilized in this work is sufficiently large, only one reacting O$_t$ every three O$_t$. The assumption is validated by enlarging the unit cell utilized, and in the p(3 × 1) unit cell the calculated absolute potential at the TS is already close to that of the IS (typically within 0.3 V). Our results are summarized in Figure 6, where the reaction barriers of the water dissociation (**1 → 2**) and the surface oxygen coupling (**1 → 9**) are plotted against the overpotential.

Figure 6 shows that the reaction barrier of water dissociation decreases linearly with the increase of overpotential. On the other hand, the barrier of the oxygen coupling reaction is rather constant over the potentials investigated. This is consistent with our recent results on Pt surfaces showing that barrier of oxygen coupling reactions (O + O and O + OH) is little affected by electric field.[19] In electrochemistry, the effect of electrochemical potential on chemical reaction is often described by an empirical linear equation E$_a$ = E$_a^0$ − αFη, which relates the barrier E$_a$ to the overpotential η.[44] E$_a^0$ is the barrier at the equilibrium potential and α is the so-called transfer coefficient. Both parameters can be determined from experiment. For OER on RuO$_2$(110) above 1.52 V, α is fitted to be 0.5 from experiment,[14] which suggests that roughly half of the work done for changing the reaction energy enters into the change of reaction barrier. From the fitted line of water dissociation reaction in Figure 6, α is 0.56, which agrees well with the experimental value.

Provided with the quantitative E$_a$∼η relation, we can deduce the theoretical Tafel line based on the classic transition state theory. The electric current

$$R \underset{k_b}{\overset{k_f}{\rightleftarrows}} O + ne^-$$
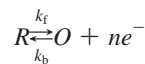
(k$_f$ ≫ k$_b$ at high overpotentials) can be expressed as follows:

$$j = nFN_A^{-1}A\exp(-\Delta G^{\#}/RT)\theta_R/S \qquad (4)$$
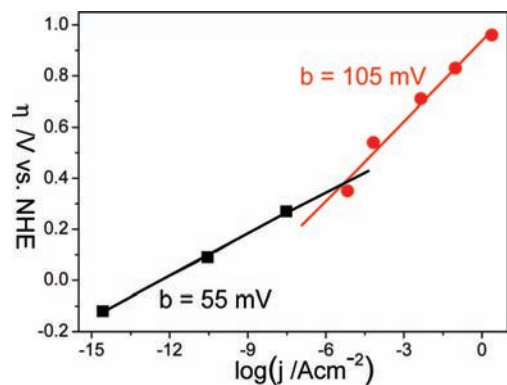
Figure 7. The calculated Tafel lines (log(j)~η plot) for OER on RuO$_2$(110). The slopes, $b = \delta\eta/\delta\log(j)$, of the fitted lines are indicated.

where A is the preexponential factor (here it is set as 10^{13}); $\Delta G^{\#}$ is the free energy barrier ($\Delta G^{\#} = E_a - T\Delta S$); θ_R is the coverage of reactive species (for the O-terminated phase, θ_R is set as 1), and S is the surface area. By utilizing the data in Figure 6, we plotted the theoretical Tafel line above 1.58 V in Figure 7, which shows that the log(j) is a linear function of the overpotential. The calculated log(j) is in a fair agreement with the experimental measurement on RuO$_2$(110), e.g., at 0.35 V overpotential, log(j) is $\sim$−4.9 from this work, and $\sim$−3.7 in experiment.[14] The slope of the Tafel line is fitted to be 105 mV, which is also close to the experiment value, 118 mV.[14]

At the potentials below 1.58 V, the electric current j is contributed from the kinetics on the OH/O mixed phase, where the overall free energy barrier is constituted by two contributions with two-electron transfer. One is from the deprotonation energy cost of the H—O$_{br}$, and the other is from the water dissociation barrier on the O-terminated surface. Since the barrier of water dissociation is found to be rather constant below 1.58 V with negative surface charges on the O-terminated phase, the deprotonation energy of H—O$_{br}$ dominates the barrier change. Adding up these two contributions, we have identified the second Tafel line below 1.58 V, which has a slope of 55 mV, as also shown in Figure 7.

Experimentally, the Tafel line at the low overpotential regime was attributed to the deprotonation of an OH being the rate-determining step in the sequential mechanism (see Introduction). According to microkinetics analysis of the sequential mechanism, the Tafel slope for the two-electron-transfer process is deduced to be 40 mV, which is however less than the experimental measurement (59 mV) on RuO$_2$(110).[14] Castelli[14] suggested that the OH might need to undergo some rearrangement before its deprotonation, which leads to the deviation of the Tafel slope. Here we provide a new mechanism at the atomic level, centering on OER on a new phase at the low overpotentials, which can exhibit a Tafel slope close to the experimental 59 mV.

With the OER kinetics on the two phases analyzed, we may address the activity of OER near the phase-transition potentials, where other H coverages ($\leq$0.33 ML H) are thermodynamically possible at finite temperatures according to Figure 1, since the H (proton/electron) exchange between the electrode surface and solution is a fast equilibrium dictated by Boltzmann distribution compared to the slow OER process. According to microkinetics, the overall rate of OER near the phase-transition potential can be deduced as $r = r_0 e^{\Delta E/RT}$, where r_0 is the OER rate on the O-terminated phase, ΔE is a potential dependent term, being the energy difference between the OH/O phases and the

O-terminated phase, $e^{\Delta E/RT}$ is thus the Boltzmann term dictating the concentration of active sites (a local O-terminated phase). As the expression is the same as that for the 0.33 ML OH/O phase, the Tafel plot in Figure 7 is unchanged.

4. Discussion

4.1. Physical Origin of Tafel Linearity. On the basis of the above results, we apparently can classify electrocatalytic reactions on surfaces into two types in general. Class I, E_a is only weakly dependent on η with a small transfer coefficient α, e.g., <0.1. Belonging to this class are the surface reactions with an LH mechanism where two adsorbed species recombine or an adsorbed species dissociates, i.e., A + B $\leftrightarrow$ AB. By checking a number of surface coupling reactions (e.g., O + O, O + OH, CO + O, H + H) studied by us and other groups[19,45−47] with different theoretical approaches, we found in general that the barrier of surface coupling reaction is insensitive to the potential. Class II, E_a is strongly dependent on η with a large α, e.g., 0.5. Class II reactions are unique to electrochemistry. Belonging to this class are the reactions with an ER-like mechanism where a coming reactant (H$_2$O itself or other species such as H$_3$O$^+$ species) from the solution reacts with the surface species, e.g., A + B + H$_2$O $\rightarrow$ AOH + BH.

To provide deeper insights into the distinct $E_a \sim \eta$ behavior of the two classes, we have examined the optimized TS structures of the water dissociation and the oxygen coupling reactions at different overpotentials. Interestingly, we found that the $E_a \sim \eta$ relation in fact coincides with the TS structural change due to the overpotential. For the water dissociation reaction, with the increase of potential, the most obvious change at the TS happens at the distance between the H of the nascent OOH complex and the O of a contacting water in the first layer water, where the H—O distance shortens from 2.09 Å ($\eta = 0.35$ V) to 1.72 Å ($\eta = 0.96$ V). While the contacting H$_2$O is polarized to stabilize the HOO—Ru$_{5c}$ complex at the TS, this stabilization effect responds positively with the increase of potential. By plotting this bond distance against overpotential, we can also identify a good linear relation as shown in Figure 8. It is noted that the central part of reaction at the TS (e.g., the dissociating OH bond) is little affected by the potential, which is in fact reasonable because the amount of added surface charge for the increase of potential is much smaller (i.e., $\sim$0.025 |e| per Ru$_{5c}$ site for $\sim$0.1 V change of η) compared to the amount of intrinsic charge transfer in the reaction. However, the potential has little effect on the TS structure of the surface oxygen coupling. The interaction between the first solvation layer and the reacting O—O complex is weak, as reflected by their long distance, $\sim$3.2 Å at all potentials investigated. The reacting O$_t$---O$_t$ bond length at the TS is always $\sim$1.65 Å. These results imply that the TS structure is a sensitive probe for the $E_a \sim \eta$ relation, in which the interaction between the first solution layer and the TS complex plays a key role.

Finally, we can answer why the water dissociation via the ER-like mechanism behaves so differently from the LH surface reactions in electrochemical conditions. With Bader charge

(44) Bard, A. J.; Faulkner, L. R. *Electrochemical Methods: Fundamentals and Applications*, 2nd ed.; John Wiley & Sons Inc.: New York, 2001.
(45) Janik, M. J.; Neurock, M. *Electrochim. Acta* **2007**, *52*, 5517.
(46) Skulason, E.; Karlberg, G. S.; Rossmeisl, J.; Bligaard, T.; Greeley, J.; Jonsson, H.; Norskov, J. K. *Phys. Chem. Chem. Phys.* **2007**, *9*, 3241.
(47) Hansen, H. A.; Rossmeisl, J.; Norskov, J. K. *Phys. Chem. Chem. Phys.* **2008**, *10*, 3722.
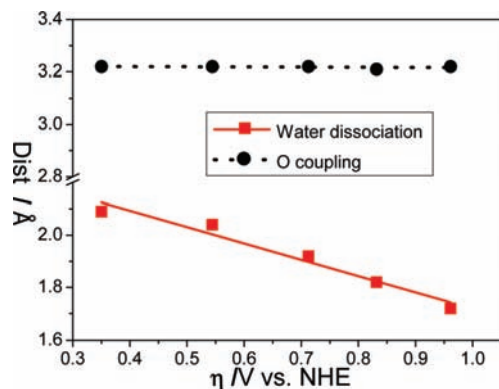
Figure 8. The shortest distance (as labeled by arrows in Figure 3) between the reacting central complex and the water layer at the TSs for the water dissociation and the surface oxygen coupling reaction on the O-terminated phase of RuO₂(110) at different overpotentials.

analysis in Table 2, we have shown that the water dissociation reaction is a redox process with electron injection from the water layer to the surface. With the elevation of potential that leads to the polarization of the water layer (the O-end of water in the first solvation layer pointing toward the surface), the TS of the water dissociation reaction can interact more strongly with the water layer, exhibiting a linear structural response to the potential (Figure 8). Because the structural response is related to the potential energy surface and the linear response should be limited in a certain regime, it is expected that the linearity in $E_a \sim \eta$ is only valid in a certain range of overpotential. For the overpotential below 0.35 V, due to already long distance (2.09 Å) between H₂O layer and the [O—OH] complex, the change of the barrier turns out to be much smaller. However, for the LH surface reactions there is no net electron transfer from the water layer to the surface. The overall effect of the potential is small due to the canceling of the solvation to the IS and the TS.

4.2. General Discussions on OER Activity. Our results show that OER occurs preferentially on the O-terminated surface, where the terminal O enables the direct splitting of H₂O with a concurrent O—OH bond formation. Since only one surface O is involved each time in the key step of OER, we can simplify the mechanism of OER as two steps: $H_2O + O_t \rightarrow O_2 + 2H^+ + 2e^-$, and $H_2O \rightarrow O_t + 2H^+ + 2e^-$. The first step dictates the high overpotential of a working OER catalyst.

From our mechanism, the differential free adsorption energy of O_t ($\delta G(O_t)$) is therefore a critical parameter for the activity, which dictates the equilibrium between H₂O in solution and the OH_x ($x = 0$ or 1) species on the surface. Since a zero $\delta G(O_t)$ would pin ΔG of $H_2O + O_t \rightarrow O_2 + 2H^+ + 2e^-$ to be zero at 1.23 V, OER would become highly activated (high overpotential) when $\delta G(O_t)$ is lower than -0.7 eV (0.7 eV is a typical free energy barrier surmountable for a reaction to occur at room temperatures with the preexponential factor $\sim 10^{13}$). However, a positive $\delta G(O_t)$ would imply the O_t on the surface is unstable on the surface and as a result the O_t may desorb as O₂ or may lead to the electrode corrosion, which is not desirable for the long-term stability.

The $\delta G(O)$ can be computed from first principles with the knowledge on surface phase diagram. In periodic slab calculations, $\delta G(O)$ is approximated by the quasi-differential oxygen free energy per additional OH_x species at a given electrochemical potential (U), as defined by eq 5.

$$\delta G(O) = G_{sur/OHx} - [G_{sur} + 1/2G_{O2} + x(G_{1/2H2} - |e|U)] \tag{5}$$

where G_{sur} is the free energy of surface before the OH_x adsorption, and the $G_{1/2H2} - |e|U$ term accounts for the free energy of H^+ and e^- via the NHE equilibrium. In order to provide a more general overview for OER across different materials, we computed $\delta G(O)$ for Pt(111),[38] RuO₂(110), and rutile IrO₂(110) and the results are compared in Figure 9. Pt surface phase diagram up to 1.4 V has been reported in our previous work.[19] For IrO₂(110), we also found three surface phases identical to those on RuO₂(110) in the range of 0.7 to 1.8 V and the phase transitions occur at 1.4 and 1.63 V.

In general, by elevating the electrochemical potential, one can increase the O coverage and at the same time destabilize the adsorbed O (thus increases $\delta G(O)$). On RuO₂(110), we found that the $\delta G(O)$ is -0.53 eV at the OH/O mixed phase ($1-1.58$ V) and it is -0.40 eV at the O-terminated phase (>1.58 V), which is within the $-0.7-0$ eV window as suggested from thermodynamics. For Pt(111) surface, $\delta G(O)$ approaches zero at about 1.2 V (0.6 ML O coverage) and further increases to 0.4 eV at 1.4 V (0.75 ML O). In fact, our previous studies showed that Pt(111) already starts to undergo surface oxidation and corrosion above 1.1 V.[38] The poor O adsorption above 1.2 V would therefore imply the material is unstable in OER conditions. However, IrO₂ tends to bind O more strongly compared to RuO₂ with $\delta G(O)$ -0.65 eV above 1.63 V at the O-terminated phase. This is consistent with the lower OER activity but higher stability for IrO₂ compared to RuO₂.[48]

The question left, interestingly, is then how to further reduce the barrier of the water dissociation on the O-terminated phase, which will expedite OER on both the OH/O mixed phase and the O-terminated phase. Theoretically, there is still a room for the reduction of barrier since the barrier of water dissociation on O_t (0.74 eV) is still higher than $-\delta G(O)$ (0.4 eV). Increasing the PH of the solution is certainly a means as already noticed in experiment,[14,49] which will help to stabilize the FS ($HOO-Ru_{5c}$ and $H-O_{br}$, both of them being acidic groups) of the water dissociation step. Doping other materials to enhance surface Os accepting H and OH from water appears to be another possible means. A simple way is to exploit a weaker O—cation bond compared to O—Ru bond, although this is usually at the expense of anode stability. This can be done with cations of lower formal oxidation states (<4+), such as Pb(2+), Ni(2+), and Co(3+) as reported in experiment.[3,7,9,11] In particular, Musiani[9] found that the addition of Pb was found to exhibit high catalytic activity with a current density 0.1 A cm⁻² at $\eta = 0.25$ V.

With the advent of DFT-MPB approach, we anticipate that the simulation of complex electrocatalytic reactions at the atomic level is now within the reach of modern computational power. The understanding of the electrocatalytic kinetics achieved in this work is beneficial for a fast screening of new anode materials in the future by focusing only on the key issues, namely, the surface phase diagram and the water dissociation step.
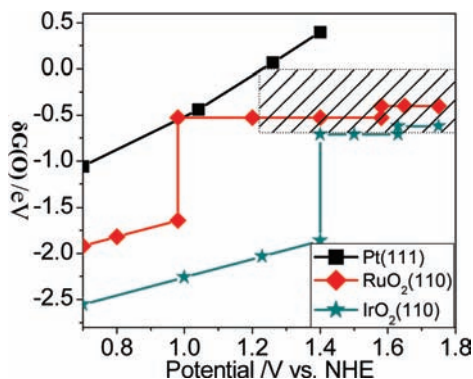
5. Conclusions

This work represents a comprehensive survey of the OER kinetics on a RuO₂(110) anode under electrochemical conditions,

(48) Kotz, R.; Stucki, S. *Electrochim. Acta* **1986**, *31*, 1311.
(49) Mohammad, A. M.; Awad, M. I.; El-Deab, M. S.; Okajima, T.; Ohsaka, T. *Electrochim. Acta* **2008**, *53*, 4351.

Figure 9. The quasi-differential oxygen free adsorption energy ($\delta G(O)$) on Pt(111), RuO$_2$(110), and IrO$_2$(110) at different electrochemical potentials. The shaded area indicates the $-0.7-0$ eV window for $\delta G(O)$ above 1.23 V.

where the periodic DFT calculations are combined with an MPB electrostatics model to take into account the effects due to the high electrochemical potential and solvation. In our approach, the slab is explicitly charged to simulate the charged electrode and the ionic distribution of the electrolyte is represented by point-charges in a continuum dielectric medium, which can be solved self-consistently. By mapping out the surface phase diagram and exploring all of the possible pathways, we identified the lowest energy reaction channels for OER above 1.23 V. Our results are detailed as follows.

(i) Above 1.58 V, the reaction occurs on the fully O-terminated phase, where each Ru$_{5c}$ is occupied by an O$_t$. The rate-determining step is the water dissociation over two Os, which leads to the concurrent O—OH bond formation.

(ii) Below 1.58 V, the reaction occurs on a OH/O mixed phase, where 0.33 ML H attaches to the O$_{br}$ and each Ru$_{5c}$ is occupied by an O$_t$. The lowest energy pathway below 1.58 V involves the conversion of the OH/O mixed phase to the O-terminated phase locally. The subsequent OER steps are exactly the same as those on the O-terminated phase above 1.58 V.

(iii) The theoretical Tafel lines are calculated with the slope fitted to be 55 and 105 mV for OER below and above 1.58 V,

respectively, where the experimental values are reported to be 59 and 118 mV with the switch at 1.52 V.

(iv) According to thermodynamics and kinetics, we deduce that the differential O adsorption energy on RuO$_2$(110) at the O-terminated phase, -0.4 eV, is within the $-0.7-0$ eV window for a good anode catalyst. Complete knowledge of both the surface phase diagram and the water dissociation kinetics is essential for the rational design of new anode catalysts.

On the basis of our results, we can classify electrocatalytic reactions into two general classes. Class I includes surface reactions with the LH mechanism, the barriers of which are insensitive to the change of potential. Class II features a coming molecule from solution to react with the surface species with the ER-like mechanism. The barrier of Class II reaction can exhibit a strong dependence on the potential. We show that the redox nature of Class II is the origin for the strong potential-dependence of the activity, where the solvation effect plays a key role in stabilizing the strongly polarized TS.

Supporting Information Available: The example showing the distribution of ionic countercharge using a DFT-MPB approach, the surface phase diagram of RuO$_2$(110) surface calculated in vacuum together with an enlarged view showing the OH/O mixed phases, convergence of k-point mesh for the calculated free energies of elementary steps, reaction barriers for oxygen coupling reactions, the MD simulation snapshots for the deprotonation of Ru$_{5c}$—OOH to solution, the optimized structures of intermediate states for OER on the OH/O mixed phase of RuO$_2$(110) at 1.4 V, and the optimized *XYZ* coordinates for key structures. This material is available free of charge via the Internet at http://pubs.acs.org.

JA1069272